



Cite this: *Nanoscale*, 2023, **15**, 5249

## Site-selective functionalization of in-plane nanoelectrode-antennas†

Maximilian Ochs, ‡<sup>a</sup> Laurent Jucker, ‡<sup>b</sup> Maximilian Rödel, <sup>c</sup> Monika Emmerling,<sup>a</sup> René Kullock,<sup>a</sup> Jens Pflaum, <sup>c</sup> Marcel Mayor \*<sup>b,d,e</sup> and Bert Hecht \*<sup>a</sup>

Stacked organic optoelectronic devices make use of electrode materials with different work functions, leading to efficient large area light emission. In contrast, lateral electrode arrangements offer the possibility to be shaped as resonant optical antennas, radiating light from subwavelength volumes. However, tailoring electronic interface properties of laterally arranged electrodes with nanoscale gaps - to e.g. optimize charge-carrier injection - is rather challenging, yet crucial for further development of highly efficient nanolight sources. Here, we demonstrate site-selective functionalization of laterally arranged micro- and nanoelectrodes by means of different self-assembled monolayers. Upon applying an electric potential across nanoscale gaps, surface-bound molecules are removed selectively from specific electrodes by oxidative desorption. Kelvin-probe force microscopy as well as photoluminescence measurements are employed to verify the success of our approach. Moreover, we obtain asymmetric current-voltage characteristics for metal-organic devices in which just one of the electrodes is coated with 1-octadecanethiol; further demonstrating the potential to tune interface properties of nanoscale objects. Our technique paves the way for laterally arranged optoelectronic devices based on selectively engineered nanoscale interfaces and in principle enables molecular assembly with defined orientation in metallic nano-gaps.

Received 12th November 2022,  
Accepted 6th February 2023

DOI: 10.1039/d2nr06343c

[rsc.li/nanoscale](http://rsc.li/nanoscale)

## Introduction

Self-assembled monolayers (SAMs) are extensively studied to introduce functionality by chemically tailoring the electronic properties of surfaces.<sup>1</sup> In case of gold surfaces, thiol-terminated alkanes and polyethylene glycols (PEGs) are among the most common SAM frameworks. While neat alkanethiols have emerged as a model system forming highly-ordered hydrophobic monolayers,<sup>2</sup> PEGs offer a less-ordered but hydrophilic pendant.<sup>3</sup> Owing to their chemical variability, SAMs offer a versatile approach to add new and advanced surface functionalities to nano- and microstructures with possible applications

ranging from biochemistry<sup>4</sup> to organic electronics.<sup>5</sup> In this context it has been shown that modifying metal electrodes with SAMs in organic light emitting diodes (OLEDs) and field-effect transistors (OFETs) is a promising strategy to reliably tune crucial properties, e.g. the Schottky-barrier height for charge carrier injection at metal-organic contact interfaces by adjusting the work function of the former and the morphology of the latter.<sup>5-7</sup> In the simplest, symmetric case both electrodes are covered by the identical SAM, but introducing asymmetry is a common method to further improve device performance by selectively promoting injection of either electrons or holes at the respective contact. In addition, the broad range of functionality offered by SAMs paves the road for advanced device concepts based on molecular switches<sup>8</sup> and machines.<sup>9,10</sup>

As the minimum droplet size in SAM deposition from liquid phase exceeds the dimensions of up-to-date's nano- and microelectrodes by far, new preparation techniques have to be implemented in order to achieve asymmetric functionalization on such small dimensions. On a comparatively large scale of several hundred micrometers, protective masks<sup>11</sup> microcontact and ink jet printing<sup>4</sup> have been employed for lateral patterning of SAMs. Significantly higher resolution is attained by dip-pen lithography or nanografting, yet tip-dependent artifacts limit this method to flat substrates.<sup>12</sup> Lithographic techniques based on the partial removal of SAM molecules include electron beam<sup>13</sup> and ultraviolet photolithography,<sup>14</sup> but neither

<sup>a</sup>NanoOptics & Biophotonics Group, Experimental Physics 5, University of Würzburg, Am Hubland, 97074 Würzburg, Germany. E-mail: [hecht@physik.uni-wuerzburg.de](mailto:hecht@physik.uni-wuerzburg.de)

<sup>b</sup>Department of Chemistry, University of Basel, St. Johannis-Ring 19, 4056 Basel, Switzerland. E-mail: [marcel.mayor@unibas.ch](mailto:marcel.mayor@unibas.ch)

<sup>c</sup>Experimental Physics 6, University of Würzburg, Am Hubland, 97074 Würzburg, Germany

<sup>d</sup>Institute for Nanotechnology (INT), Karlsruhe Institute of Technology (KIT), P.O. Box 3640, 76021 Karlsruhe, Germany

<sup>e</sup>Lehn Institute of Functional Materials (LIFM), School of Chemistry, Sun Yat-Sen University (SYSU), Guangzhou 510275, China

†Electronic supplementary information (ESI) available: Additional measurements and discussion thereof, KPFM correction, symmetric metal-organic nanoantennas. See DOI: <https://doi.org/10.1039/d2nr06343c>

‡These authors contributed equally to this work.



has been used to fabricate functional devices. In another approach, molecules are desorbed from laser-excited plasmonic nanostructures *via* hot-electron mediated gold-sulfur cleavage.<sup>15</sup> While in principle allowing for functionalization at sub-particle resolution, the need for plasmonic resonances and homogeneous illumination limits this technique to small areas of specific device geometries. In addition, a sophisticated laser setup is required.

As most optoelectronic devices are inherently electrically connected, the electrochemical desorption in a cyclic voltammetry (CV) cell offers a simple and direct way to remove SAMs from gold surfaces.<sup>16–20</sup> Oxidative as well as reductive desorption have been investigated, but the latter is more frequently used and benefits from its straightforward reaction, involving one electron per thiol molecule. This method has since been extended to coat substrates with different SAMs and scaled down to electrode distances below the optical diffraction limit as verified by Kelvin probe force microscopy (KPFM).<sup>21,22</sup> In pursuit of even smaller electronic and optoelectronic devices,

however, there exists a great demand for techniques that selectively address individual electrodes of nanoscale extensions and spacings of only a few tens of nanometers, while preserving the delicate nature of these nanostructures. Confirming the success of such functionalization with the required nanometer resolution constitutes a major challenge.

Here, we demonstrate an easy-to-use technique for nanoscale site-selective functionalization of arbitrarily shaped laterally arranged nanoelectrodes with different types of SAMs. As substrates we use standard microelectrodes as well as electrically-connected optical nanoantennas of different geometries.<sup>23,24</sup> Both are fabricated from chemically grown mono-crystalline (111) gold platelets, which serve as a platform for advanced nanoscale optoelectronic devices, *via* focused ion beam milling.<sup>25,26</sup> Our SAM adsorption procedure is sketched in Fig. 1. We do not use sophisticated electronic or optical setups, instead our technique is based on oxidative desorption of alkyl and PEG thiols in a droplet of electrolyte. In contrast to the usually employed reduction where thiol anchoring

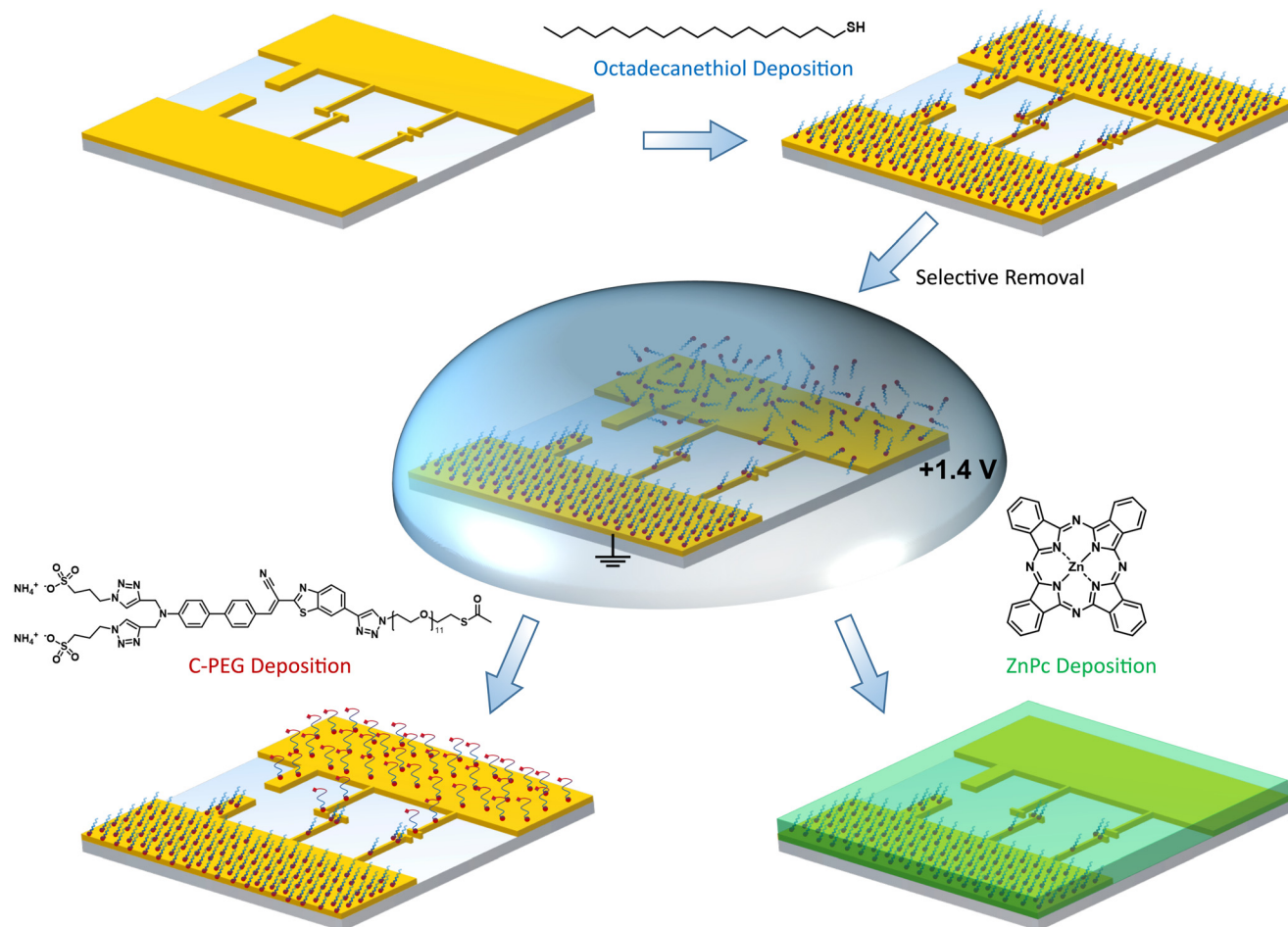


**Fig. 1** Illustration of site-selective functionalization. First, the sample (with different micro- and nanoelectrodes) is completely covered with 1-octadecanethiol (C18-SH). Then, a droplet of KOH/*n*-butanol is applied and molecules are removed from the biased electrode *via* oxidative desorption. A different SAM, e.g. a chromophore containing PEG (C-PEG), is deposited on the liberated electrode, while the C18-SH SAM still covering the opposite electrode acts as a blocking layer. Alternatively, an organic semiconductor, here zinc phthalocyanine, is evaporated onto the asymmetric antenna arrangement to study interface modifications introduced by C18-SH.



groups are removed as thiolates, the oxidative removal leads to sulfates and sulfonates according to the following reactions:



As the oxidized species have a considerably reduced affinity to gold surfaces, the method is less prone to issues and artifacts arising from readsorbed molecules.<sup>27–29</sup> This is the key feature for nano-sized objects, as already a few readsorbed molecules might have a strong impact on the overall surface properties. By utilizing the steric hindrance imposed by long-chain alkanethiols, such as 1-octadecanethiol (C18-SH), a second SAM based *e.g.* on a chromophore containing PEG (C-PEG) is deposited on the stripped/uncovered electrode. In order to verify the successful site-selective functionalization, we map the surface coverage by KPFM and photoluminescence measurements. In addition, we demonstrate that the electronic properties of metal–organic interfaces can be tuned on the nanoscale by assembling a functionalized hybrid antenna structure covered by the prototypical organic semiconductor zinc phthalocyanine (ZnPc). Our technique enables the fabrication of nano-optoelectronic devices with advanced functionalities and oriented molecular assemblies, aiming for the overall goal to integrate molecular machinery into metallic nanoelectrodes.

## Results and discussion

In Fig. 2a, the asymmetric functionalization of a plasmonic nanoantenna by site-selective removal of a chemisorbed SAM is illustrated. A representative SEM image is shown in Fig. 2b comprising a pair of electrically connected arms separated by

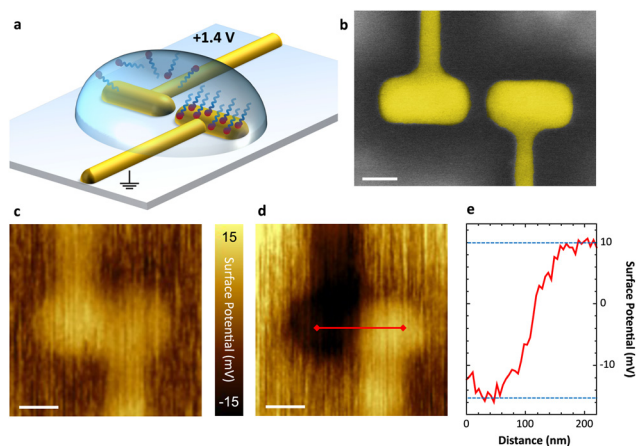


**Fig. 2** Oxidative desorption at the nanoscale. (a) Schematic of molecule removal from one arm of an electrically-connected nanoantenna upon applying +1.4 V in KOH/*n*-butanol. (b) SEM image of an exemplary plasmonic nanoantenna with a gap of 30 nm. Scale bar 50 nm. (c) and (d) KPFM images of a plasmonic nanoantenna (c) after deposition of C18-SH and (d) after selectively removing the SAM from the left arm. Scale bars 100 nm. The fast scan direction is bottom to top. (e) Cross-section along the red line in (d) showing an effective surface potential (SP) difference of 25 mV between the two antenna arms.

a 30 nm gap, whose wiring allows us to apply a voltage between both nanoelectrodes. In a first step, C18-SH, known as a reference for densely packed SAM formation,<sup>2</sup> is deposited onto the gold surface from ethanolic solution. For the selective electrochemical removal of the SAM, 0.1 mM solution of potassium hydroxide (KOH) in *n*-butanol is drop-casted on the sample and a DC voltage of +1.4 V is applied to the left antenna electrode for 30 s. As a result, the gold–thiol bonds on this electrode are broken<sup>16</sup> and the released molecules are rinsed off with ethanol, while the SAM covering the opposite antenna electrode remains intact and firmly bound. As desorbed molecules may remain close to the surface,<sup>18,27</sup> the rinsing step is crucial and the solvent should be adjusted to fit the SAM's polarity and solubility. The applied voltage can be cycled to improve overall removal of molecules; however, the associated risk of gold surface oxidation may lead to inferior adsorption of a second SAM.

In order to verify the site-selective functionalization at the nanoscale, we look for the modification of the surface dipole upon adsorption of the SAM. This change is dominated by the effective interface dipole moment of the monolayer (with negligible contribution from the gold–sulfur interaction) which is determined by the strength and orientation of the molecules' dipole moment and the SAM density. An altered surface dipole will lead to a shift of the vacuum energy level and, thus, an increase or decrease of the gold–SAM electrode work function, depending on the direction of the SAM dipole moment. For example, CH<sub>3</sub>-terminated alkanethiols reduce the work function (compared to a pure gold (111) surface) as their dipole points towards the surface, while their CF<sub>3</sub>-terminated analogues lead to the opposite effect.<sup>7,30–32</sup> We are able to observe and to qualify this effect with KPFM, which maps the effective surface potential (SP) - a measure correlated to the work function difference of sample and probe tip.<sup>21</sup> This allows us to measure variations induced by different molecular coverage.

KPFM images of an antenna before and after site-selective desorption of molecules is shown in Fig. 2c and d. Both antenna arms have the same effective SP after deposition of a homogeneous C18-SH SAM (see Fig. 2c). Upon selective removal from the left antenna arm, KPFM reveals a clear contrast (see Fig. 2d). In this case a nominal SP difference of 25 mV between the two electrodes can be observed (see Fig. 2e). This indicates that only the right antenna electrode and its connector are still covered by an intact SAM. We note that the measured shift is far below values measured by ultraviolet-photoelectron spectroscopy in vacuum.<sup>33</sup> This is attributed to the following experimental challenges: (I) the large size of the platinum–iridium KPFM probe tip limits spatial resolution and measurable SP contrast. The 50 nm diameter of the tip is larger than the antenna gap, and thus the tip collects signal from both antenna electrodes while scanning across the gap. (II) Imaging is carried out under ambient conditions; hence, a water layer forms on the uncovered gold surface and induces a dipole moment, which is parallel to the SAM dipole on the covered gold surface.<sup>34</sup> (III) The antenna surface is not perfectly flat after focused ion beam milling, which leads to



distortion of the SAM in respect of packing and alignment. While the last two points cannot be discriminated in our current setup, we account for probe related artifacts by calibration. A set of known voltages is applied across the electrodes during KPFM and, thereby, we obtain a corrected SP contrast of 200 mV for asymmetric functionalization with C18-SH (see ESI†). We believe this to be the upper limit for measuring SP contrast in this experiment due to the influence of water adsorption and non-perfect surface topographies.

As our method allowed for simple and selective removal of C18-SH SAMs from micro- and nanoscopic electrodes, we were eager to investigate its applicability towards more complex molecules. The highly hydrophilic C-PEG which combines the well-studied PEG chains with a chromophore was chosen as a suitable candidate for this purpose (see Fig. 1).<sup>35</sup> A dodecaethyleneglycol chain with a protected terminal thiol group is intended to act as an anchor to the gold (111) surface. The long chain ensures sufficient emitter-metal distance and minimizes quenching once the molecules are immobilized upright standing on the gold.<sup>36</sup> The dye can be excited at 532 nm and has a broad emission in the red spectral regime. By using C-PEG, we obtain an optical feedback on larger microelectrodes *via* fluorescence and can demonstrate that most molecules are removed from the surface upon oxidative desorption.

In order to immobilize C-PEG on the gold surface, it is dissolved in methanol and the masked thiols are deprotected by adding a droplet of 5.4 M NaOMe solution. Next, the substrate is immersed in the solution for 20 minutes resulting in a homogeneous light-emitting SAM in the subsequent PL

studies. In Fig. 3a, the direct removal of C-PEG is demonstrated for a substrate with two microscopic electrodes milled into a mono-crystalline gold (111) platelet. C-PEG desorption from the top electrode is carried out as described above for C18-SH, but 0.1 mM KOH in water is used to ensure the solubility of C-PEG. Next, we record a hyperspectral photoluminescence (PL) map showing almost no light emission from that electrode surface, verifying that the C-PEG SAM is indeed removed, while PL is still observed from the opposite electrode. Some molecules remain at the edges of the stripped electrode owing to the large amount of surface defects. In addition, we observe a small unintended desorption from the other gold electrode surface. This is attributed to unstable SAM formation of the PEG chains and hence, solvents with high affinity for the molecules, *e.g.* dimethyl sulfoxide and water can easily wash the SAM away (even without applied voltage). Still, this method is suitable for the removal of hydrophilic molecules; even at the nanoscale as shown in the ESI.†

In order to protect C-PEG against any other solvent, we modified the procedure: First, C18-SH is deposited onto the substrate and selectively removed from one of the electrodes. Next, we add C-PEG as described above. Consequently, C18-SH acts as a blocking layer and our target molecule mainly binds to the uncovered electrode. As depicted in Fig. 3b, this method results in a high-quality, unperturbed SAM with homogeneous light emission on the bottom electrode of a second sample. The other electrode, instead, is still covered with C18-SH, and thus almost no emission from the flat surface is observed. Spectra directly extracted from the hyperspectral PL maps

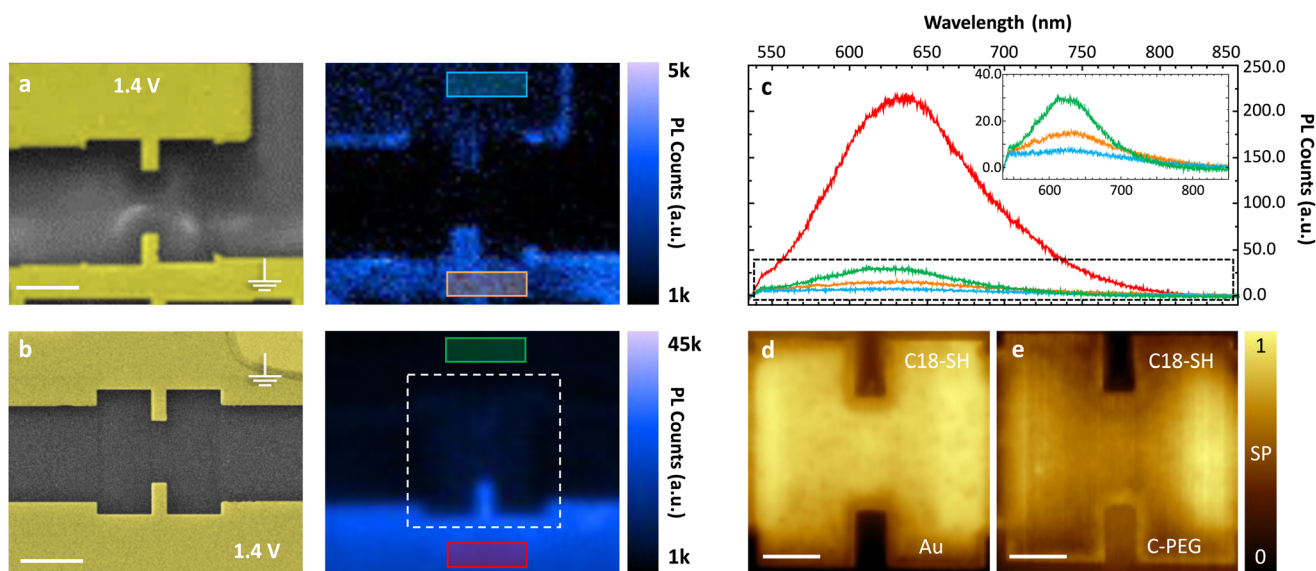


**Fig. 3** Site-selective functionalization with light-emitting SAM. (a) and (b), Left: SEM images of two microelectrodes. Right: Hyperspectral PL maps of the same electrodes after selective functionalization. Each pixel contains a spectrum, which is integrated to give the total PL counts. Scale bars 2  $\mu\text{m}$ . (a) Direct desorption of C-PEG. After molecule deposition, a DC voltage of +1.4 V is applied to the top electrode, while the other electrodes are grounded. (b) C18-SH is first deposited as a blocking layer and selectively removed by applying +1.4 V to the bottom electrode. Subsequently, C-PEG is deposited and binds to the bottom electrode. (c) Measured spectra recorded by averaging all pixels in the colored rectangles of (a) and (b). The inset shows a zoom into the spectra (black dashed rectangle). (d) and (e) Normalized KPFM images of the marked area in (b; white rectangle) taken (d) after site-selective desorption of C18-SH and (e) after subsequent deposition of C-PEG on the liberated electrode. The surface coverage is denoted. Scale bars 1  $\mu\text{m}$ .



allow for further comparison between the two approaches for site-selective functionalization (see Fig. 3c). Minimal light emission from the surface covered with C18-SH is detected (green) as a result of competitive SAM formation. However, emission from the surface without blocking layer (red) is much stronger and significantly exceeds the one obtained in Fig. 3a, indicating that direct removal leads to partial desorption of the C-PEG SAM at the opposite electrode. To further verify the homogeneous coverage of surfaces with C18-SH and C-PEG, we record KPFM maps of an exemplary stripe-electrode. The image in Fig. 3d is taken after removing the blocking layer and displays the expected uniform contrast between covered and uncovered electrode surfaces. This contrast is reversed upon formation of the subsequent C-PEG SAM (see Fig. 3e) owing to its strong dipole moment. We can deduce that the latter is oriented parallel to the dipole moment of C18-SH and has a larger absolute value, thus leading to a stronger SP shift.<sup>30,31,33</sup>

According to these results we conclude that (I) a significant portion of alkanethiol molecules is removed upon oxidative desorption; (II) the use of a blocking layer is beneficial, and therefore the preferred method for asymmetric functionalization by unstable SAMs, which can easily be desorbed from the surface (e.g. C-PEG); (III) the very low electrolyte concentration does not noticeably oxidize the surface as this would

hamper the formation of an additional SAM and (IV) an unintended SAM removal *via* reductive desorption is not observed.

Next, we demonstrate the feasibility to selectively modify metal–organic interfaces in a nanoscale device. A schematic of the structure and an exemplary SEM image are depicted in Fig. 4a. We employ a stack arrangement similar to that in organic light emitting antennas (OLEAs)<sup>24</sup> and functionalize only one of the electrodes by C18-SH. Finally, we vacuum deposit a 30 nm thick layer of the organic semiconductor zinc phthalocyanine (ZnPc; green) on top of the antenna configuration. ZnPc grains around and atop the antenna are visible in the SEM image. The resulting energy diagram for the antenna electrodes with and without C18-SH is illustrated in Fig. 4b. Note, ZnPc deposited on clean gold (111) surfaces, e.g. the stripped antenna electrode, is characterized by preferential hole injection due to the smaller injection barrier.<sup>24</sup> As mentioned before, the presence of the alkanethiol SAM shifts the vacuum energy at the Au-SAM-ZnPc boundary and consequently lowers HOMO and LUMO levels relative to the metal work function. In contrast, the stripped (uncovered) electrode experiences only a small shift of the vacuum energy due to a weaker interface dipole at the Au-ZnPc boundary. Hence, the antenna electrodes exhibit selectively modified injection barriers for electrons and holes. The change in morphology of

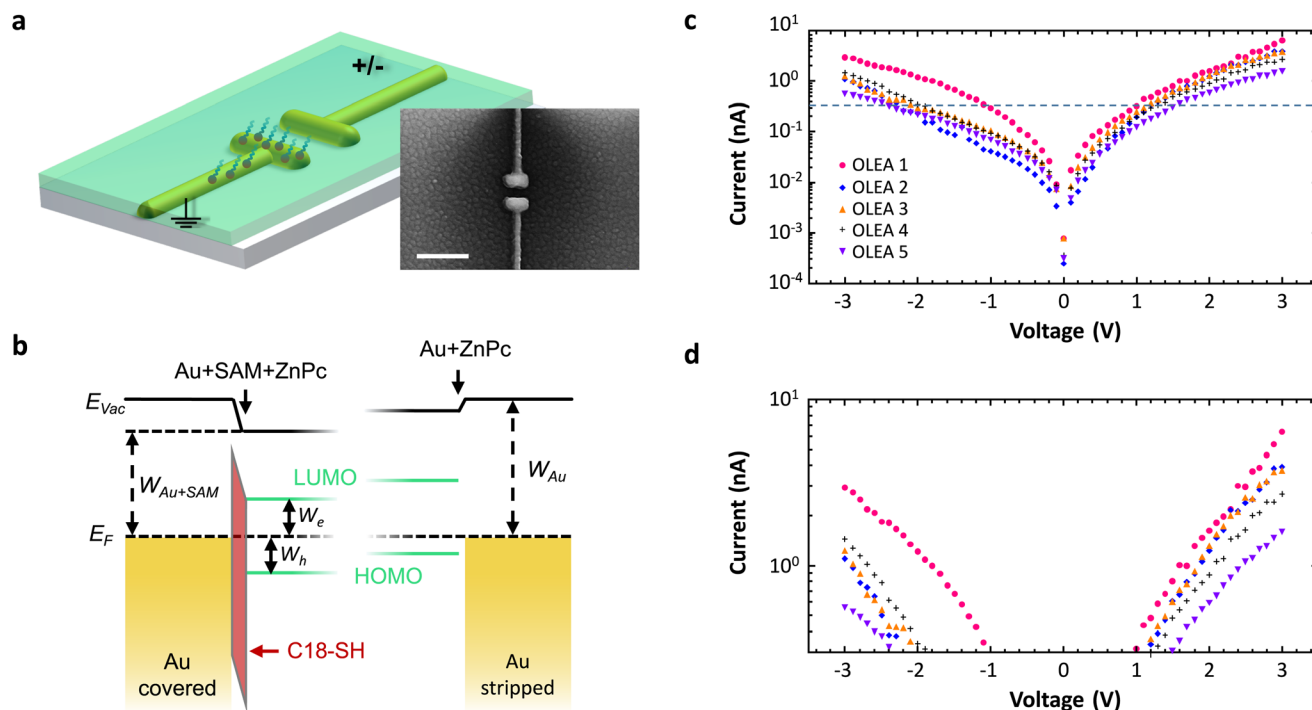


**Fig. 4** Tuning the gold-organic interface. (a) Schematic of metal–organic nanoantenna with asymmetric functionalization. After C18-SH is removed from one electrode, ZnPc (green) is evaporated. Inset: SEM image of a finalized antenna structure. The bottom arm is covered with C18-SH. The granular texture of the film is caused by ZnPc domains formed upon deposition. Scale bar 300 nm. (b) Energy diagram of the two electrodes with and without C18-SH SAM. ZnPc evaporated on clean gold exhibits a smaller injection barrier for holes than for electrons. The interface dipole introduced by the SAM shifts the vacuum energy level  $E_{vac}$  and lowers the HOMO and LUMO levels relative to the metal work function  $W_{Au}$  (identified by the Fermi energy  $E_F$ ). As a consequence, injection barriers for electrons ( $W_e$ ) and holes ( $W_h$ ) are selectively modified. Note, the Au-ZnPc boundary also exhibits a small interface dipole. (c) Absolute current as a function of applied voltage for five different devices (with similar dimensions). (d) Zoom-in to the region above the dashed line in (c). The higher currents obtained for positive voltages indicate the asymmetric injection behavior of the selectively functionalized antenna contacts. In all measurements, the SAM-functionalized electrode is grounded.



ZnPc grown on top of a SAM covered electrode *versus* that on a pure gold surface can further influence charge carrier injection.<sup>5</sup> We investigate the effect of asymmetric functionalization by recording current–voltage characteristics of several devices. In these measurements, functionalized electrodes are grounded and the voltage is applied to the stripped antenna arm (*cf.* Fig. 4a). As shown in Fig. 4c and d, all five devices exhibit asymmetric *IV*-curves, *i.e.* higher currents at positive voltages, which is in line with a reduced injection barrier for electrons and an increased injection barrier for holes at the SAM-functionalized antenna electrode. Small current variations for different antennas are attributed to slight variations at the metal–organic boundaries. On the other hand, antennas featuring SAMs on both electrodes have symmetric *IV*-curves (see ESI†). Hence, this experiment is a further proof that we can selectively cover specific nanoscale electrodes and thereby tune the electronic and presumably also structural interface properties of more advanced nanodevices.

## Conclusions

In summary, we demonstrated an easy-to-use and straightforward technique for site-selective functionalization of micro- and nanoelectrodes with ultra-small dimensions, such as optical antennas. Instead of relying on complicated optical setups, our technique is based on simple oxidative desorption making use of the low probability for readsorption. Surfaces are covered with C18-SH as well as fluorescent C-PEG and asymmetric functionalization is carried out either by direct removal of the previously chemisorbed SAM or by using C18-SH as a blocking layer. The latter is especially beneficial for SAMs which are unstable upon exposure to a highly affine solvent. KPFM and photoluminescence measurements confirm that a significant portion of molecules is desorbed without strongly oxidizing the gold surface. Additionally, we apply our method to selectively modify interface properties of metal–organic nanoantennas, further demonstrating the potential for future nano-optoelectronic devices. By using SAMs with tailored dipole moments and even photoswitchable units,<sup>8,38,39</sup> the precise engineering of structural as well as electronic interface properties of nanoscale objects seems feasible in the future. This might pave the road not only towards functional (opto-)electronic nanodevices, but also to the integration of artificial molecular machinery between metallic nanoelectrodes. Once immobilized with a clearly defined orientation, such molecules can perform defined and directed motions controlled by the nanoelectrodes.<sup>35</sup>

## Experimental

### Materials and methods

**Sample preparation.** Au/Cr electrode structures (70 nm/5 nm thickness) are fabricated *via* optical lithography and electron

beam physical vapor deposition. Mono-crystalline gold platelets are chemically grown on glass cover slips (#1, Gerhard Menzel GmbH), transferred to the electrodes, and structured by FIB milling (Helios Nanolab, FEI Company; acceleration voltage of 30 kV).<sup>23,25,26</sup> In order to remove gold debris after milling, an etching solution of I<sub>2</sub> : KI : H<sub>2</sub>O = 1 mg : 4 mg : 40 ml is applied for 20 s and washed away with purified water and ethanol.<sup>37</sup> Before molecules are deposited, all samples are rinsed in isopropanol.

SAMs of octadecanethiol are prepared by adding 12 mg of molecules (O1858, Sigma-Aldrich) to 15 mL of absolute ethanol. After the mixture is sonicated for ten minutes, the sample is immersed in the solution and the container is back-filled with nitrogen. The typical incubation time is 24 hours. Eventually, the sample is taken out of the solution, rinsed with absolute ethanol (to remove excess molecules) and dried with a stream of nitrogen.

SAMs of C-PEG are prepared by adding a few grains of molecules to 2 mL of methanol. The solution is sonicated until all molecules are dissolved. In order to deprotect the thiol group, one droplet of sodium methoxide (5.4 M, Acros Organics) is added and the sample is immersed immediately for 20 minutes. Afterwards, the sample is rinsed with purified water and dried with a stream of nitrogen.

ZnPc is evaporated at a rate of 10–15 Ångström per minute (controlled *via* quartz crystal oscillator) in a high-vacuum multi-chamber system that operates at a base pressure of 10<sup>−8</sup> mbar.

**Electrical Setup.** Desorption of molecules as well as current–voltage measurements are carried out using the same source measure unit (Keithley 2636B, Keithley Instruments Inc.). Electrodes are contacted by micromanipulators (DPP220, FormFactor) that are equipped with Copper-beryllium probe needles (MM-7H, Micromanipulator).

**Kelvin probe force microscopy measurements.** Maps are recorded using a Horiba AIST-NT CombiScope-1000 SPM equipped with PPP-NCHPt conductive probes (Nanosensors; PT/Ir coating, frequency = 330 kHz, radius < 25 nm). Scanning is done in tapping mode with scan rates of 0.2–0.4 Hz with a lift height of 30 nm. All measurements are carried out under ambient conditions at room temperature.

**Photoluminescence measurements.** Optical measurements are conducted with an inverted confocal microscope. Light from a 532 nm laser diode (AIST-NT ROU006) is reflected by a dichroic mirror (Thorlabs Di01-R532) and focused on the top-side of the sample using a 50x air objective (Olympus MPlanFLN; NA = 0.8). Photoluminescence is recorded by the same objective, filtered (Semrock LP03–532RS-25) and analyzed by a spectrometer (Horiba iHR 320, 150 lines mm<sup>−1</sup>) in combination with an electron-multiplied charge-coupled device (Andor Newton 970P EMCCD). In order to acquire hyperspectral maps, the sample stage is scanned relative to the laser spot and a spectrum is measured at each pixel. The integration time per pixel is 20 ms and the laser power in front of the objective is 500 μW.



## Author contributions

M. O. and L. J. conceived the individual experiments. M. E. fabricated evaporated electrode structures and transferred gold platelets. M.O. fabricated optical nanoantennas as well as microelectrodes. L. J. synthesized C-PEG. M. O. performed site-selective functionalization, KPFM, photoluminescence and current–voltage measurements. M. R. vacuum deposited ZnPc. M. O., L. J., J. P., M. M. and B. H. analyzed the data and co-wrote the manuscript. R. K., J. P., M. M. and B. H. supervised the project.

## Conflicts of interest

There are no conflicts to declare.

## Acknowledgements

Generous financial support by the Volkswagen-Stiftung (Az. 93438) as well as by the German Research Foundation (projects HE 5618/8-1 and PF385/12-1) is acknowledged. J.P. appreciates financial support by the Bavarian State Ministry of Science, Research, and the Arts (Collaborative Research Network “Solar Technologies Go Hybrid”).

## References

- 1 F. Schreiber, *Prog. Surf. Sci.*, 2000, **65**, 151–257.
- 2 C. Vericat, M. E. Vela, G. Benitez, P. Carro and R. C. Salvarezza, *Chem. Soc. Rev.*, 2010, **39**, 1805–1834.
- 3 Y. J. Du and J. L. Brash, *J. Appl. Polym. Sci.*, 2003, **90**, 594–607.
- 4 J. C. Love, L. A. Estroff, J. K. Kriebel, R. G. Nuzzo and G. M. Whitesides, *Chem. Rev.*, 2005, **105**, 1103–1170.
- 5 S. Casalini, C. A. Bortolotti, F. Leonardi and F. Biscarini, *Chem. Soc. Rev.*, 2017, **46**, 40–71.
- 6 P. Stoliar, R. Kshirsagar, M. Massi, P. Annibale, C. Albonetti, D. M. de Leeuw and F. Biscarini, *J. Am. Chem. Soc.*, 2007, **129**, 6477–6484.
- 7 B. de Boer, A. Hadipour, M. M. Mandoc, T. van Woudenberg and P. W. M. Blom, *Adv. Mater.*, 2005, **17**, 621–625.
- 8 M. A. Bartucci, J. Florián and J. W. Ciszek, *J. Phys. Chem. C*, 2013, **117**, 19471–19476.
- 9 S. Erbas-Cakmak, D. A. Leigh, C. T. McTernan and A. L. Nussbaumer, *Chem. Rev.*, 2015, **115**, 10081–10206.
- 10 I. Aprahamian, *ACS Cent. Sci.*, 2020, **6**, 347–358.
- 11 T. Mosciatti, P. Greco, T. Leydecker, M. Eredia, F. Biscarini and P. Samori, *ACS Omega*, 2017, **2**, 3502–3508.
- 12 R. D. Piner, J. Zhu, F. Xu, S. Hong and C. A. Mirkin, *Science*, 1999, **283**, 661–663.
- 13 J. Rundqvist, J. H. Hoh and D. B. Haviland, *Langmuir*, 2006, **22**, 5100–5107.
- 14 S. Friebel, J. Aizenberg, S. Abad and P. Wiltzius, *Appl. Phys. Lett.*, 2000, **77**, 2406–2408.
- 15 S. Simoncelli, Y. Li, E. Cortés and S. A. Maier, *ACS Nano*, 2018, **12**, 2184–2192.
- 16 C. A. Widrig, C. Chung and M. D. Porter, *J. Electroanal. Chem. Interfacial Electrochem.*, 1991, **310**, 335–359.
- 17 T. Kawaguchi, H. Yasuda, K. Shimazu and M. D. Porter, *Langmuir*, 2000, **16**, 9830–9840.
- 18 E. Pensa, C. Vericat, D. Grumelli, R. C. Salvarezza, S. H. Park, G. S. Longo, I. Szleifer and L. P. M. D. Leo, *Phys. Chem. Chem. Phys.*, 2012, **14**, 12355–12367.
- 19 E. H. J. Wong, G. L. May and C. P. Wilde, *Electrochim. Acta*, 2013, **109**, 67–74.
- 20 M. Tencer and P. Berini, *Langmuir*, 2008, **24**, 12097–12101.
- 21 A. Liscio, E. Orgiu, J. M. Mativetsky, V. Palermo and P. Samori, *Adv. Mater.*, 2010, **22**, 5018–5023.
- 22 C. Wälti, R. Wirtz, W. A. Germishuizen, D. M. D. Bailey, M. Pepper, A. P. J. Middelberg and A. G. Davies, *Langmuir*, 2003, **19**, 981–984.
- 23 J. Kern, R. Kullock, J. Prangma, M. Emmerling, M. Kamp and B. Hecht, *Nat. Photonics*, 2015, **9**, 582–586.
- 24 P. Grimm, S. Zeißner, M. Rödel, S. Wiegand, S. Hammer, M. Emmerling, E. Schatz, R. Kullock, J. Pflaum and B. Hecht, *Nano Lett.*, 2022, **22**, 1032–1038.
- 25 E. Krauss, R. Kullock, X. Wu, P. Geisler, N. Lundt, M. Kamp and B. Hecht, *Cryst. Growth Des.*, 2018, **18**, 1297–1302.
- 26 X. Wu, R. Kullock, E. Krauss and B. Hecht, *Cryst. Res. Technol.*, 2015, **50**, 595–602.
- 27 A. Musgrove, A. Kell and D. Bizzotto, *Langmuir*, 2008, **24**, 7881–7888.
- 28 R. L. Garrell, J. E. Chadwick, D. L. Severance, N. A. McDonald and D. C. Myles, *J. Am. Chem. Soc.*, 1995, **117**, 11563–11571.
- 29 M. H. Schoenfish and J. E. Pemberton, *J. Am. Chem. Soc.*, 1998, **120**, 4502–4513.
- 30 P. C. Rusu and G. Brocks, *J. Phys. Chem. B*, 2006, **110**, 22628–22634.
- 31 R. W. Zehner, B. F. Parsons, R. P. Hsung and L. R. Sita, *Langmuir*, 1999, **15**, 1121–1127.
- 32 J. Pflaum, G. Bracco, F. Schreiber, R. Colorado, O. E. Shmakova, T. R. Lee, G. Scoles and A. Kahn, *Surf. Sci.*, 2002, **498**, 89–104.
- 33 D. M. Alloway, M. Hofmann, D. L. Smith, N. E. Gruhn, A. L. Graham, R. Colorado, V. H. Wysocki, T. R. Lee, P. A. Lee and N. R. Armstrong, *J. Phys. Chem. B*, 2003, **107**, 11690–11699.
- 34 R. L. Wells and T. Fort, *Surf. Sci.*, 1972, **32**, 554–560.
- 35 L. Jucker, M. Ochs, R. Kullock, Y. Aeschi, B. Hecht and M. Mayor, *Org. Mater.*, 2022, **4**, 127–136.
- 36 Y. S. Chi, H. R. Byon, B. S. Lee, B. Kong, H. C. Choi and I. S. Choi, *Adv. Funct. Mater.*, 2008, **18**, 3395–3402.
- 37 R. Kullock, M. Ochs, P. Grimm, M. Emmerling and B. Hecht, *Nat. Commun.*, 2020, **11**, 115.
- 38 N. Crivillers, S. Osella, C. Van Dyck, G. M. Lazzerini, D. Cornil, A. Liscio, F. Di Stasio, S. Mian, O. Fenwick,



- F. Reinders, M. Neuburger, E. Treossi, M. Mayor, V. Palermo, F. Cacialli, J. Cornil and P. Samorì, *Adv. Mater.*, 2013, **25**, 432–436.
- 39 D. A. Egger, F. Rissner, G. M. Rangger, O. T. Hofmann, L. Wittwer, G. Heimel and E. Zojer, *Phys. Chem. Chem. Phys.*, 2010, **12**, 4291–4294.

